The Planar Parabolic Optical Antenna

David T. Schoen,[1,2] Toon Coenen,[2] F. Javier García de Abajo[3], Mark L. Brongersma,[1] and

Albert Polman[2]*

[1]Stanford University, CA, USA

[2]Center for Nanophotonics, FOM Institute AMOLF

Science Park 104, 1098 XG, Amsterdam, The Netherlands

[3]IQFR-CSIC, Serrano 119, 28006 Madrid, Spain

ABSTRACT One of the simplest and most common structures used for directing light in macroscale applications is the parabolic reflector. Parabolic reflectors are ubiquitous in many technologies, from satellite dishes to handheld flashlights. Today, there is a growing interest in the use of ultra-compact metallic structures for manipulating light on the wavelength scale. Significant progress has been made in scaling radiowave antennas to the nanoscale for operation in the visible range, but similar scaling of parabolic reflectors employing ray-optics concepts has not yet been accomplished because of the difficulty in fabricating nanoscale three-dimensional surfaces. Here, we demonstrate that plasmon physics can be employed to realize a resonant elliptical cavity functioning as an essentially planar nanometallic structure that serves as a broadband unidirectional parabolic antenna at optical frequencies.

KEYWORDS: Plasmonics, Nanophotonics, Cathodoluminescence, Optical Antennas

Controlling the far field emission pattern of nanoscale objects is one of the central goals of optical antennas[1,2]. In most cases, the desired pattern is a beam of light in the far field, which can couple a nanoscale source or sink of light to a distant object. Optical beaming could improve performance in a variety of important applications, such as photon sources[3], photodetectors[4], sensors[5] and photovoltaics[6]. Previous antennas have demonstrated beaming into engineered directions over narrow frequency ranges[7-12], or broadband beaming in structures several times larger the wavelength[13], however a broadband device with a small footprint and high directivity has not yet been demonstrated. Parabolic reflectors are ubiquitous macroscopic structures that efficiently couple electromagnetic energy from a focal point to a beam, and work over a very large range of frequencies. It would seem natural that parabolic structures would also be useful for small-scale optical antennas: however, fabricating complex three-dimensional surfaces is not generally possible with traditional nanofabrication tools. By using a gold surface as a 2 dimensional medium for propagation of surface waves, namely surface plasmon polaritons, it is possible to reduce the dimensionality of a parabolic reflector while maintaining its optical beaming behavior. We demonstrate that a two dimensional cross-section of a paraboloid cut into a gold surface, namely a resonant elliptical cavity, presents the broadband unidirectional emission expected of the full three dimensional structure and is much more amenable to fabrication. When reduced in size to the wavelength-scale these structures retain their beaming functionality and also present a set of well defined optical resonances that enhance emission for particular wavelengths.
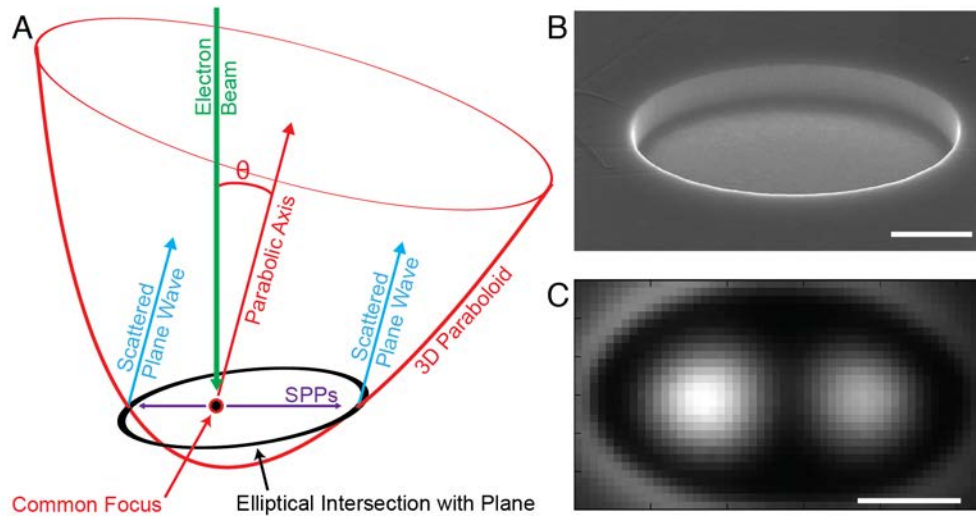
Figure 1: Elliptical cavity antenna design, realization, and operation. A) Schematic of the intersection of a paraboloid with a planar surface, creating an ellipse. B) SEM image of elliptical arena taken at 52° off the surface normal. The scale bar is 500 nm. C) 30 keV cathodoluminescence image at a collection wavelength of 720 nm for a 1.0-μm long, 800-nm wide elliptical cavity. Scale bar is 250 nm.

Parabolic reflectors are well known in geometrical optics; they couple the emission of a point source at the parabolas' focus to a plane wave propagating parallel to parabola's axis, and *vice versa*. In a classical three-dimensional parabola the emitted light beam originates from the specular reflection of light over the entire parabola's surface. However, due to the special geometrical properties of a parabola, an array of individual scatterers placed in a parabolic arrangement will also generate a parallel beam of light in the far field. In fact, a point source coupled to any two-dimensional sub-section of a paraboloidal surface will generate a wave preferentially propagating parallel to the paraboloid's axis. One special case of such a sub-section is the elliptical intersection of a paraboloid with a planar surface, with the paraboloid and the planar ellipse sharing a common focus. In such a geometry, a beam of light can be generated by exciting surface plasmon polaritons (SPPs) near one of the two foci inside the planar ellipse

followed by coherent scattering of the SPP to free-space photons via the edges of the area in the form of a collimated beam. The direction of the beam is only determined by the position of the source inside the ellipse and the ellipse's eccentricity. Figure 1a shows this geometry. A detailed analytic description of this model is given in the Supplementary Information. A series of concentric elliptical groves has recently been used to realize a bull's eye type beam director with a controllable beam direction based on a similar concept[14]. In contrast to this work, the elliptical bull's eye structure has a well-defined operation wavelength based on coherent scattering from multiple groves, whereas here the broad optical resonances of the plasmonic cavity are utilized to achieve high directivities.

The elliptical arenas were fabricated by focused ion beam (FIB) milling using an FEI Helios Nanolab Dual Beam instrument into a single crystal pellet of gold which had been previously polished to nanometer-scale roughness. Similar geometries can also be made using template stripping.[15,16] Patterns were defined as bitmaps and milled top to bottom with a beam current of 1.5 pA. Higher beam currents also provide structures with similar behavior. Cathodoluminescence (CL) data were collected in a FEI XL-30 SFEG SEM with a custom-made parabolic mirror mounted on a 4 axis piezo-driven alignment system to accurately position the planar ellipsoidal cavities in the focus of the half-paraboidal collection mirror in the SEM. 2D images of the light emitted by the collection mirror were collected on a Pixis CCD and this data was mathematically transformed into the angle-resolved maps shown in Figure 4. Spectra were collected by directing the light into a fiber-coupled spectrometer.

A scanning electron microscopy (SEM) image of a characteristic ellipse is shown in Fig. 1b. Several different elliptical geometries were fabricated with major axes lengths ranging between 500 and 1600 nm, and eccentricities, defined as the ratio between the major axis length and the

focus-to-focus distance, between 0 and 1. The depth of the elliptical cavity was also varied; typically a depth of 400 nm was used. The localized optical modes in these structures were determined using our newly developed angle-resolved cathodoluminescence imaging spectroscopy (ARCIS) technique. A 30 keV electron beam is raster-scanned over the surface and serves as a broad-band point source of surface plasmon polaritons. The radiation spectrum emitted by the antenna is collected by a half-paraboloidal mirror (focal length 0.5 mm) placed between the microscope's pole piece and the sample. In parallel, the angular distribution of the emitted light is recorded by collecting the light beam emanating from the collection paraboloid on a two-dimensional CCD camera[17,18]. Figure 1c shows a cathodoluminescence (CL) image of a 1000×600 nm elliptical cavity recorded at a wavelength of 720 nm. The pixel size in the images of the smaller cavities is 10×10 nm, and it is 20×20 nm in the largest cavities. The two foci of the elliptical antenna are clearly resolved in the image, demonstrating the subwavelength resolution of the CL technique. As CL is a direct probe of the radiative component of the local density of optical states (LDOS),[19] images such as in Fig. 1c provide a direct absolute measure of the radiation power of the antenna at any wavelength.

Figure 2 shows CL images for cavities with an eccentricity of 0.8, with major axes between 500 nm and 1.6 μm. Data are shown for collection wavelengths in the range 550-935 nm. As can be seen, as the ratio of cavity size to wavelength increases, cavity modal intensity distributions of increasing mode order are observed. Modal distributions of a similar type have previously been observed in plasmonic whispering gallery cavities and cylindrical cavities,[16,20] and the modal distributions of photonic elliptical cavities has been explored by near-field scanning optical microscopy[21,22]. Figure 3 shows the CL spectra averaged over the elliptical cavity area for the 2D scans presented in Fig. 2. It can be seen that the resonant modes shift to longer wavelengths as

the cavities increase in size. Different resonant modes, observed in Fig. 2, appear as different resonant peaks in the spectra. The quality factor for the plasmon resonances in Fig. 2 is in the range Q=10-20. Larger cavities have lower quality factors due to increased ohmic losses of the SPPs in the metal. Resonant modes at long wavelengths have lower Q due to a lower reflection coefficient at the cavity end, caused by a larger modal evanescent tail in the normal direction into the air. Similarly, deeper cavities show higher quality factors due to increased reflectivity of the metallic walls, which lowers the radiation losses (Supplementary Fig. 1).
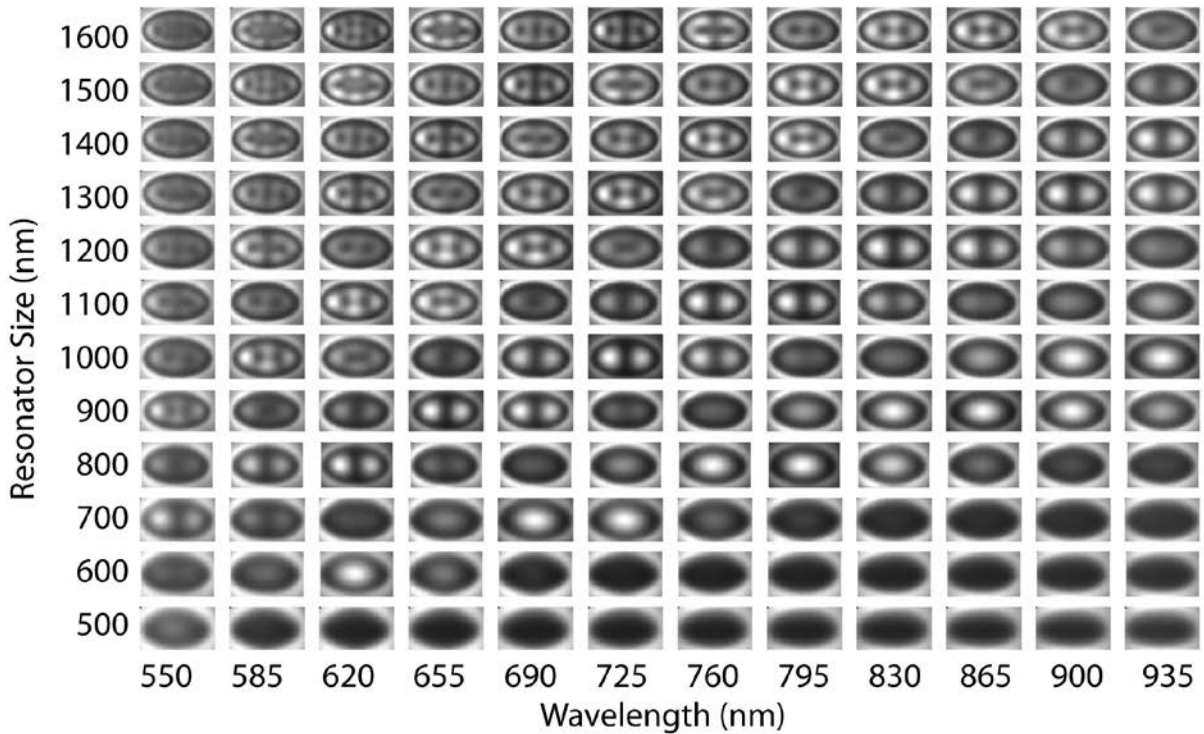

Figure 2. Experimental elliptical cavity modal intensity distributions. Cathodoluminescence images (30 keV electrons) for cavities with eccentricity 0.8 and major axes ranging from 500 nm to 1600 nm for different collection wavelengths. Cavity modal patterns with increasing mode order (m=0,1,2, …) are clearly visible. All images are scaled by the major axis length.

While an exact analysis of the elliptical cavities resonant modes can be made using a Green's function approach or the boundary-element method,[21-23] a first-order model that provides very good physical insight predicts resonances occurring when the phase accumulated by surface plasmon polaritons travelling a round trip inside the ellipse is equal to an integer number m times 2π:

$$2Lk_{spp} + 2\phi = 2m\pi, \quad (1)$$

with L the major axis length, k_{spp} the SPP wave vector, and ϕ the phase increment upon reflection at the cavity boundary. This model very well describes the cavity modes in one-dimensional nanowires where the resonance are determined by the cavity length.[24-27] All the experimentally observed peaks can be fit with this model, even though it only considers resonances related to one characteristic length, that of the major axis. This directly follows from the special geometrical properties of ellipses: in an elliptical cavity, in a simple ray optics picture, all rays that emanate from one focus will reflect off the ellipse's edge in the direction of the opposite focus. The distance of this path is the same regardless of the initial direction of the first ray, and is equal to the major axis length. Thus the major axis length defines the characteristic resonances for the cavity. The reflections of SPPs in elliptical cavities have been explored previously by leakage radiation microscopy for large cavities with major axis lengths greater than 30 μm[28], but this is the first time such a model has been proposed for a resonant SPP cavity on the wavelength-scale. We approximate the SPP wave vector by that for an SPP propagating on an infinite plane of gold. The wave vector in the ellipse will be affected by the lateral confinement imposed by the walls of the cavity, which explains the shift observed between the predicted peak positions and those in the experiment. The increased confinement

Interestingly we do not see spectral evidence of any whispering gallery type modes. It is possible that such modes, if they exist, are confined to the corners of the structure. If so, they will have a mode index substantially higher than those for the SPPs propagating on the floor of the cavity, and thus may radiate poorly to the far field.
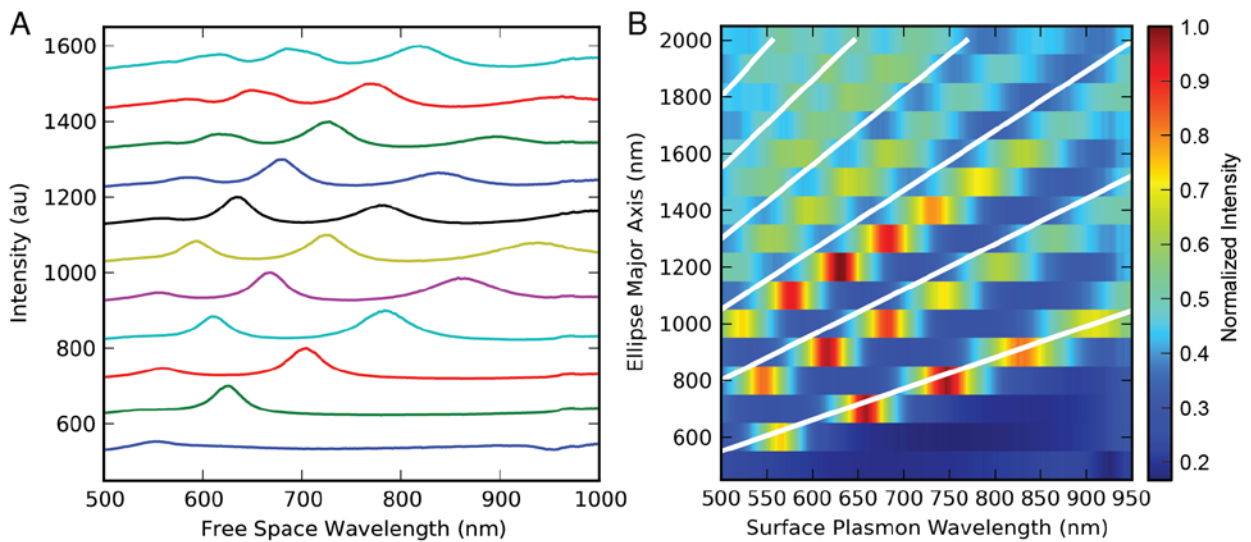

Figure 3. Experimental elliptical cavity mode spectra. A) Cathodoluminescence spectra for elliptical cavities with eccentricity 0.8 with major axes ranging from 500 nm to 1600 nm. A redshift for the various resonances increasing cavity size is clearly visible. B) Same data as in (A) now represented in a map of CL intensity versus surface plasmon wavelength and cavity major axis. The white lines indicate the resonant modes calculated using a Fabry-Perot interference model.
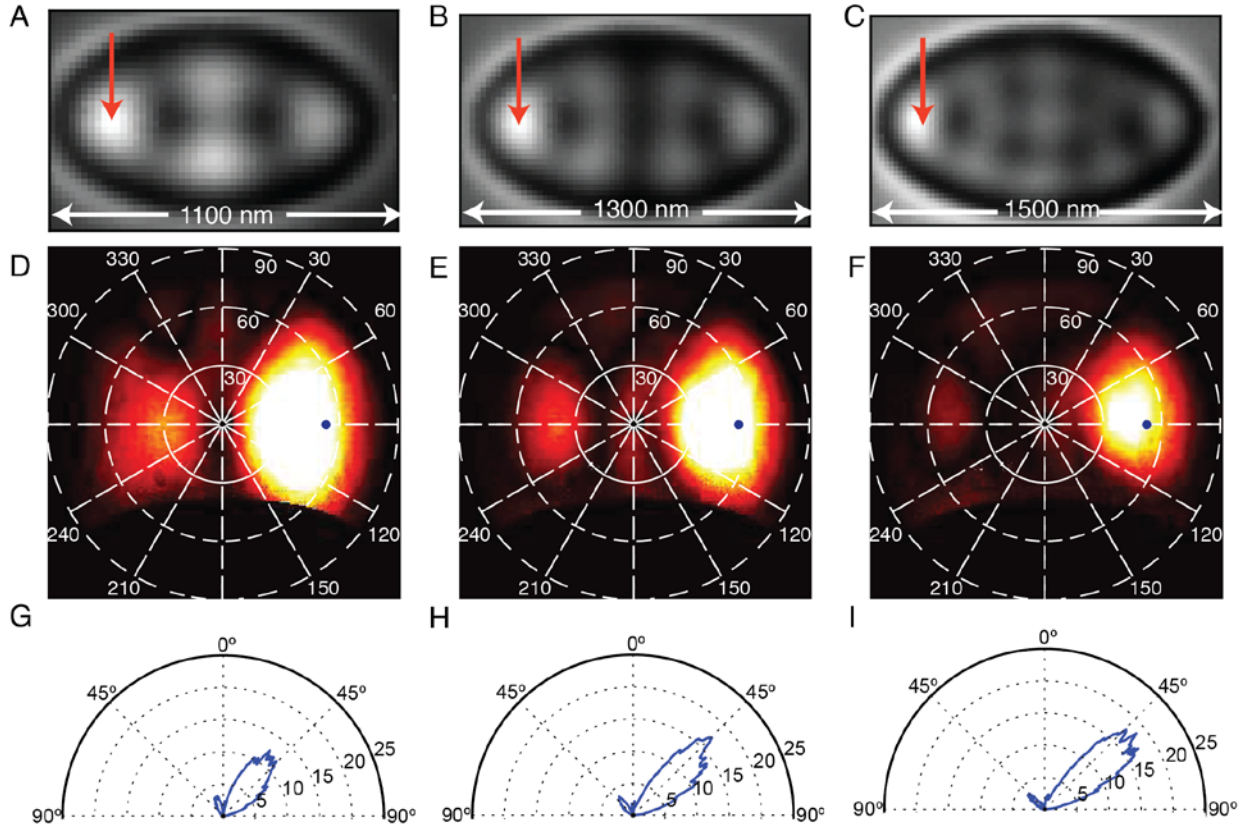
Figure 4. Strong light beaming from elliptical antennas. A-C) CL images of elliptical antennas with eccentricity 0.8 and major axes of 1100, 1300, and 1500 nm taken at resonance wavelengths of 628 nm, 609 nm, and 589 nm, respectively. The images are scaled by the major axis length. D-F) Normalized angular emission collected using a 40 nm band pass filter centered at 600 nm for the three cavities. taken using electron beam excitation at the modal maxima in (A) (see arrows). Blue dots indicate the paraboloid axis for each structure. G-I). Line cuts at the azumithal angle of peak emission with the data normalized as directivity. The maximum directivity in panel (I) is 18

Figure 3b shows the data from Fig. 3a replotted versus plasmon wavelength and cavity length. The linear resonance redshift with cavity length is clearly visible (see also Supplementary Fig. 2a). We fitted equation (1) through the entire data set for all modes in Fig. 3b, with the phase

pickup ϕ as the only free parameter, which yields the white dashed lines in Fig. 3b. The model describes the overall trends very well (see also Supplementary Fig. 2b) and yields $\phi = -1.2\pi$. The negative value obtained for ϕ is in contrast to experiments on strip antennas which have shown a positive phase pickup.[24,29] The negative phase pickup for an SP reflecting of the metallic ellipse boundary is similar in nature to the negative phase pickup seen for a plane wave reflection off a metal mirror. This phase shift effectively makes the arena appear smaller than would be expected for a phase pickup $\phi=0$. This attenuation in the spatial extent of the modes is also clearly visible in the modal distributions in Fig. 2, in which a band of low CL signal is observed on the inside edges of the cavities for all modes and cavity sizes.

Figure 4 shows the angular distribution of light emitted by the cavities in terms of the directivity at these angles. The directivity of an antenna is related to an antenna's ability to radiate light in a particular direction

$$D(\theta, \phi) = \frac{4\pi}{P_{rad}} p(\theta, \phi) \quad (2)$$

Where the directivity D is given as a function of azimuthal and zenithal angle and is proportional to the emitted power p at these angles normalized by the total radiated power P_{rad} per solid angle. Data are shown for elliptical cavities with eccentricity of 0.8 and major axes of 1.1 μm, 1.3 μm, and 1.5 μm. Figures 4a-c show the CL intensity maps for the resonances nearest 600 nm for each cavity: at 628 nm, 609 nm, and 589 nm, respectively. Figures 4d-f show the angular emission patterns collected for e-beam excitation of the antenna in the outermost antinode in the resonant modal intensity pattern. Clear beaming of light of these resonant modes at an azimuthal angle φ=90° and zenithal angle θ=52° is observed. Our model predicts the angle to be 53.1° for this eccentricity, in reasonable agreement. The smallest half-width-at-half-maximum (HWHM) is found in the largest cavity: 17° and 24° for the azimuthal and zenithal angles respectively.

Figure 4g-i shows cuts of the angular emission distribution in the zenithal angular emission lobe, with the radial scale plotted as emission directivity, i.e. the emission normalized by an isotropic emitter of the same total power. We find that the maximum observed directivity is 18.0 for the 1.5 μm antenna. This value compares favorably to other near wavelength scale devices, such as the nanoscale Yagi Uda antenna[10], but is clearly lower than structures that are larger in size such as the bull's eye directors[9]. This tradeoff is evident in our own observation that larger structures give higher directivities. In the end there will always be a tradeoff between absolute size and the maximum achievable directivity related to the diffraction of the emitted light.

The data in Fig. 4 clearly show the strong directivity of the elliptical antenna, a unique feature given its planar geometry. It is the result of the constructive interference in the far-field of surface plasmon polaritons that are coherently scattered off the boundary of the elliptical cavity. The operation wavelength and outcoupling angle can be tuned by varying the ellipses' geometrical size and eccentricity (Supplementary Fig. 3). The main emission peaking near $\theta=53°$ observed in Fig. 4 corresponds well to the optical axis of a paraboloid intersecting with the gold surface, with the focal point at the position of the electron beam impact, as indicated in Fig. 4a. E-beam illumination of the area around the foci which appear bright in the LDOS map (4a-c) leads to a 'forward' directed beam in the far field (Supplementary Fig. 4). This work thus provides a demonstration of the coupling of the two-dimensional optical "flatland" with the three-dimensional far-field. A central advantage of this type of antenna is that every resonant mode directs energy in the same direction, as can be observed for the three modes in Fig. 4. In contrast, many other antenna designs will only broadcast in the 'forward' direction for a single designed frequency. In this sense, the antenna is 'broadband.' Of course, strong LDOS enhancement is only available when the structure is on resonance, so the most accurate

description is that the antenna has several operating bands, each of which broadcasts energy in the forward direction. Since this is a plasmonic cavity with a moderate Q, these bands are not narrow, but have a bandwidth of about 50 nm and are tunable by varying the size of the ellipse. Another distinct feature of these elliptical antennas is that the volume from which emitters can couple is relatively large, i.e. on the order of a wavelength cubed. This can be contrasted with the Yagi Uda antenna composed of an array of coupled metal nanoparticles.[7,10,18] Such an antenna (which shows a similar angular spread as the elliptical antennas presented here) has an approximately two-orders-orders-of-magnitude smaller volume from which emitters can efficiently couple to the antenna's radiation field as that is determined by the optical near-field of one metal nanoparticle, typically a shell with a thickness of only ~20 nm around the "feed" particle (Supplementary Information). In many applications where precise positioning of the local emitter is impossible or difficult, this will be a significant advantage. Furthermore, taking advantage of the fact that SPPs can be excited electrically,[30] and the fact that electrical circuitry can be integrated with the planar antenna geometry, this design may pave the way for electrically driven directional optical antenna emitters. Finally we note the application of these elliptical antennas in the receiving mode, e.g. in photodetectors and solar cells, in which light with different colors can be selectively collected and converted to electrical current at distinct regions inside the cavity.

In conclusion, we have demonstrated a novel antenna design, a resonant elliptical cavity, that enables the controlled coupling of optical emitters to the far-field at a well-defined angle. The emission is due to the excitation and coherent scattering of surface plasmon polaritons to the far field, at optical resonances with Q=10-20. The cavity has strong directivity (18.0) and has a corresponding optical volume that is more than 100 times larger than that of an optical Yagi Uda

antenna. The direction and wavelength of operation of the antenna can be controlled by simple geometric parameters. This work demonstrates the possibility of integrating 'flatland' optics with the far-field, namely the control of three-dimensional electromagnetic radiation by two-dimensional resonant structures, and can lead to important applications in a large variety of technology areas, including lighting, photodetectors, quantum optical circuitry, and photovoltaics.

ASSOCIATED CONTENT

Supporting Information. An appendix describing analytically the parabolic scattering model. Several supplementary figures presenting data on resonator linewidth vs cavity depth, the extraction of the phase pickup on reflection, angular radiation patterns as a function of cavity eccentricity, and total forward directivity vs beam position. The calculation of the effective coupling model. This material is available free of charge via the Internet at http://pubs.acs.org

AUTHOR INFORMATION

Corresponding Author

*email: a.polman@amolf.nl

Author Contributions

DS, MB, TC, and AP conceived and designed the experiments. DS and TC carried out fabrication and characterization of the antenna structures. DS and TS analyzed the collected data. All authors contributed to the writing and preparation of the manuscript.
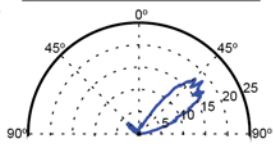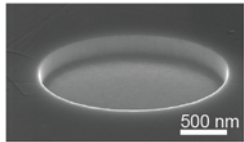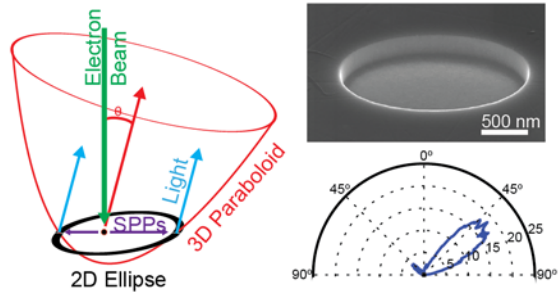
REFERENCES

1.   Novotny, L.; van Hulst, N. Antennas for Light. *Nat. Photonics* **2011**, *5*, 83–90.
2.   Bharadwaj, P.; Deustsch, B.; Novotny, L. Optical Antennas. *Adv. Opt. Photonics* **2009**, *1*, 438–483.
3.   Yu, N.; Fan, J.; Wang, Q. J.; Pflügl, C.; Diehl, L.; Edamura, T.; Yamanishi, M.; Kan, H.; Capasso, F. Small-Divergence Semiconductor Lasers by Plasmonic Collimation. *Nat. Photonics* **2008**, *2*, 564–570.
4.   Tang, L.; Kocabas, S. E.; Latif, S.; Okyay, A. K.; Ly-Gagnon, D.-S.; Saraswat, K. C.; Miller, D. A. B. Nanometre-Scale Germanium Photodetector Enhanced by a Near-Infrared Dipole Antenna. *Nat. Photonics* **2008**, *2*, 226–229.
5.   Taminiau, T. H.; Moerland, R. J.; Segerink, F. B.; Kuipers, L.; van Hulst, N. F. Λ/4 Resonance of an Optical Monopole Antenna Probed by Single Molecule Fluorescence. *Nano Lett.* **2007**, *7*, 28–33.
6.   Atwater, J. H.; Spinelli, P.; Kost, E.; Parsons, J.; Van Lare, C.; Van De Groep, J.; Garcia de Abajo, J.; Polman, A.; Atwater, H. A. Microphotonic Parabolic Light Directors Fabricated by Two-Photon Lithography. **2011**, 1–4.
7.   de Waele, R.; Koenderink, A. F.; Polman, A. Tunable Nanoscale Localization of Energy on Plasmon Particle Arrays. *Nano Lett.* **2007**, *7*, 2004–2008.
8.   Jun, Y. C.; Huang, K. C. Y.; Brongersma, M. L. Plasmonic Beaming and Active Control Over Fluorescent Emission. *Nat. Comm.* **2011**, *2/4*, 283–6.
9.   Lezec, H. J.; Degiron, A.; Devaux, E.; Linke, R. A.; Martín-Moreno, L.; Garcia-Vidal, F. J.; Ebbesen, T. W. Beaming Light From a Subwavelength Aperture. *Science* **2002**, *297*, 820–822.
10.   Curto, A. G.; Volpe, G.; Taminiau, T. H.; Kreuzer, M. P.; Quidant, R.; van Hulst, N. F. Unidirectional Emission of a Quantum Dot Coupled to a Nanoantenna. *Science* **2010**, *329*, 930–933.
11.   Han, S.; Norris, D. Beaming Thermal Emission From Hot Metallic Bull's Eyes. *Opt. Express* **2010**, *18*, 4829–4837.
12.   Dregely, D.; Taubert, R.; ller, J. D. U.; Vogelgesang, R.; Kern, K.; Giessen, H. 3D Optical Yagi-Uda Nanoantenna Array. *Nat. Comm.* **2011**, *2*, 271–7.
13.   Shegai, T.; Miljkovic, V. D.; Bao, K.; Xu, H.; Nordlander, P.; Johansson, P.; Käll, M. Unidirectional Broadband Light Emission From Supported Plasmonic Nanowires. *Nano Lett.* **2011**, *11*, 706–711.
14.   Tetienne, J. P.; Blanchard, R.; Yu, N.; Genevet, P.; Kats, M. A.; Fan, J. A.; Edamura, T.; Furuta, S.; Yamanishi, M.; Capasso, F. Dipolar Modeling and Experimental Demonstration of Multi-Beam Plasmonic Collimators. *New Journal of Physics* **2011**, *13*, 053057.

15. Nagpal, P.; Lindquist, N. C.; Oh, S. H.; Norris, D. J. Ultrasmooth Patterned Metals for Plasmonics and Metamaterials. *Science* **2009**, *325*, 594–597.

16. Vesseur, E. J. R.; Polman, A. Plasmonic Whispering Gallery Cavities as Optical Nanoantennas. *Nano Lett.* **2011**, *11*, 5524–5530.

17. Coenen, T.; Vesseur, E. J.; Polman, A. Angle-Resolved Cathodoluminescence Spectroscopy. *Appl. Phys. Lett.* **2011**, *99*, 1–4.

18. Coenen, T.; Vesseur, E. J. R.; Polman, A.; Koenderink, A. F. Directional Emission From Plasmonic Yagi–Uda Antennas Probed by Angle-Resolved Cathodoluminescence Spectroscopy. *Nano Lett.* **2011**, *11*, 3779–3784.

19. Garcia de Abajo, F. J. Optical Excitations in Electron Microscopy. *Rev. Mod. Phys.* **2010**, *82*, 209–275.

20. Zhu, X.; Zhang, J.; Xu, J.; Li, H.; Wu, X.; Liao, Z.; Zhao, Q.; Yu, D. Dispersion Control in Plasmonic Open Nanocavities. *ACS nano* **2011**, *5*, 6546–6552.

21. Chicanne, C.; David, T.; Quidant, R.; Weeber, J.; Lacroute, Y.; Bourillot, E.; Dereux, A.; Colas des Francs, G.; Girard, C. Imaging the Local Density of States of Optical Corrals. *Phys. Rev. Lett.* **2002**, *88*, 97402.

22. Babayan, Y.; McMahon, J.; Li, S.; Gray, S.; Schatz, G.; Odom, T. Confining Standing Waves in Optical Corrals. *ACS nano* **2009**, *3*, 615–620.

23. Colas des Francs, G.; Girard, C.; Weeber, J.; Chicane, C.; David, T.; Dereux, A.; Peyrade, D. Optical Analogy to Electronic Quantum Corrals. *Phys. Rev. Lett.* **2001**, *86*, 4950–4953.

24. Barnard, E.; White, J.; Chandran, A.; Brongersma, M. Spectral Properties of Plasmonic Resonator Antennas. *Opt. Express* **2008**, *16*, 16529–16537.

25. Søndergaard, T.; Bozhevolnyi, S. I. Strip and Gap Plasmon Polariton Optical Resonators. *Physica Status Solidi (b)* **2008**, *245*, 9–19.

26. Novotny, L. Effective Wavelength Scaling for Optical Antennas. *Phys. Rev. Lett.* **2007**, *98*.

27. Vesseur, E. J. R.; de Waele, R.; Lezec, H. J.; Atwater, H. A.; Garcie de Abajo, F. J.; Polman, A. Surface Plasmon Polariton Modes in a Single-Crystal Au Nanoresonator Fabricated Using Focused-Ion-Beam Milling. *Appl. Phys. Lett.* **2008**, *92*, 083110.

28. Drezet, A.; Stepanov, A. L.; Ditlbacher, H.; Hohenau, A.; Steinberger, B.; Aussenegg, F. R.; Leitner, A.; Krenn, J. R. Surface Plasmon Propagation in an Elliptical Corral. *Appl. Phys. Lett.* **2005**, *86*, 074104.

29. Barnard, E. S.; Coenen, T.; Vesseur, E. J. R.; Polman, A.; Brongersma, M. L. Imaging the Hidden Modes of Ultrathin Plasmonic Strip Antennas by Cathodoluminescence. *Nano Lett.* **2011**, *11*, 4265–4269.

30. Walters, R. J.; Loon, R. V. A. V.; Brunets, I.; Schmitz, J.; Polman, A. A Silicon-Based Electrical Source of Surface Plasmon Polaritons. *Nat. Mater.* **2009**, *9*, 21–25.

TABLE OF CONTENTS FIGURE:

Electron
Beam

θ

Light

Light

3D Paraboloid

SPPs

2D Ellipse

500 nm

0°

45°   45°

                            25
                       20
                    15
              10
          5

90°   90°

Planar parabolic optical antennas

D.T. Schoen,[1,2] **T. Coenen,**[2] **F.J. García de Abajo**[3]**, M. L. Brongersma,**[1] **and A. Polman**[2]

[1]Stanford University, CA, USA
[2]Center for Nanophotonics, FOM Institute AMOLF
Science Park 104, 1098 XG, Amsterdam, The Netherlands
[3]Institute of Optics, Serrano 121, 28006 Madrid, Spain

The Virtual Parabola Model for the Beaming of an Elliptical Cavity.

There are five statements made in the manuscript text that can be demonstrated with a simple geometry.

(1) A 3D paraboloid will satisfy the condition that all paths from a focus, to a point on the paraboloid, to a plane normal to the paraboloid's axis, will have the same distance.

(2) A planar cross section of this surface that includes the focal point and is normal to the paraboloid axis is a circle.

(3) A similar cross section that includes the focal point for a paraboloid whose axis is rotated by angle θ from the normal is an ellipse.

(4) One focus of the ellipse is coincident with the paraboloid's focus.

(5) The eccentricity of this ellipse is determined only by the angle θ.
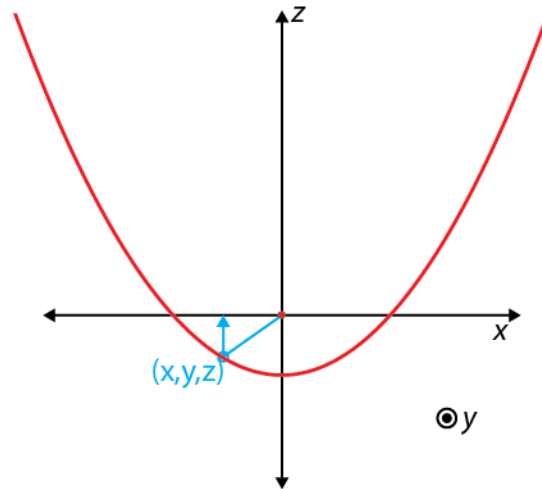


Supplementary Scheme 1: **A parabola in the x-z plane**

We can rephrase statement (1) as the equation below for a 3-dimensional paraboloid:

$$\sqrt{x^2 + y^2 + z^2} - z = d \ \ [1],$$

where the term in the radical is the distance from the origin to some point on the parabolic surface *x,y,z*, and *z* is the distance from that point to a plane, arbitrarily chosen to be the *x-y* plane. To meet the condition of statement (1), this quantity must equal a constant, which is arbitrary, here represented by *d*. This equation can be easily reordered into the following form:

$$z = \frac{1}{2d}(x^2 + y^2) - \frac{d}{2} \ [2].$$

This is the equation of a paraboloid with its focus at the origin and its vertex at (0,0,-*d*/2). Again, we can emphasize that the choice of *d* is arbitrary, any d will satisfy equation [1] and therefore statement (1). Note that the important condition for beaming is not *path length,* which is what we have considered here, but rather *phase propagation,* which must take into account the path length as well as the wave vector. That more general case will also be considered, but for the elliptical cavity antenna the mode index is very close to 1, so the simple geometric argument is approximately correct.
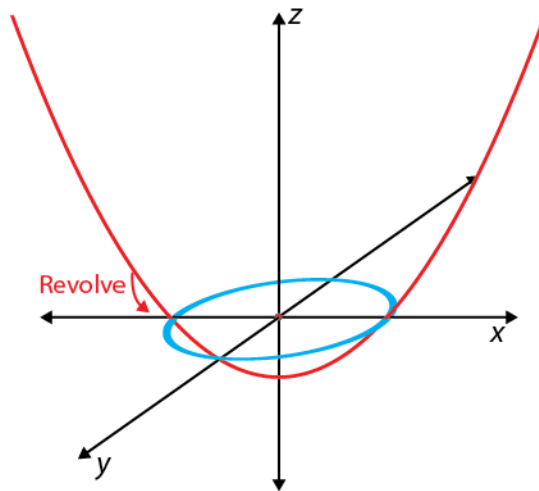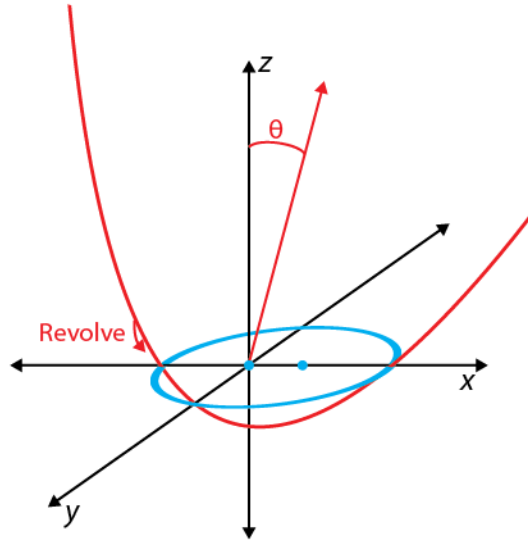

Supplementary Scheme 2: **A 3D paraboloid intersects the *x-y* plane to form a circle.**

In order to illustrate statement (2) we need only to consider the intersection of this shape with the *x-y* plane, which by definition contains the focus of the parabola at (0,0,0) This is given by equation [2] where the value of *z* is set to zero:

$$x^2 + y^2 = d^2 \ [3].$$

Here we have the simple result that this intersection is just a circle, centered at the origin, with radius *d*. This demonstrates that a circle will scatter light emitted from its center in the normal direction. Another way to think of this would be as a bull's eye type structure with a single groove, which should serve as a broadband director oriented normal to the surface.

In order to illustrate statement (3), it is necessary to introduce a simple coordinate rotation. Now consider a similar ellipsoid in the x', y', z' coordinate system, which is rotated in the x-z plane by an angle θ:

Supplementary Scheme 3: **A tilted 3D paraboloid intersects the x-y plane to form an ellipse.**

$$z' = \frac{1}{2d}(x'^2 + y'^2 - d^2) \ [4].$$
$$y' = y$$
$$x' = x\cos\theta - z\sin\theta$$
$$z' = x\sin\theta + z\cos\theta$$
$$x'^2 = x^2\cos^2\theta + z^2\sin^2\theta - 2xz\sin\theta\cos\theta$$

We are once again interested in the intersection of the paraboloid described in the x',y',z' coordinate system with the x-y plane. In this case $z = 0$:
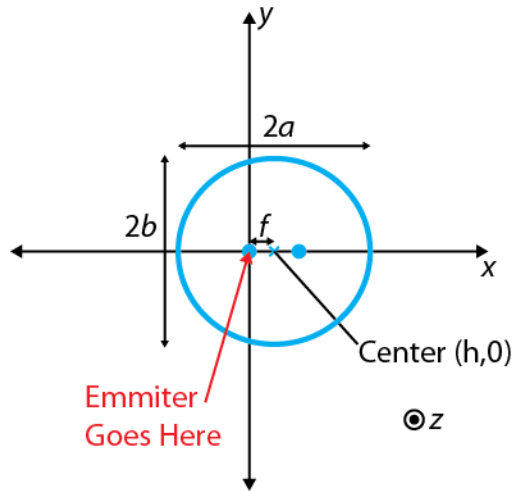
$$x\sin\theta = \frac{1}{2d}(x^2\cos^2\theta + y^2 - d^2) \ [5].$$

Now we need only gather up terms and rewrite the equation to reveal the ellipse:

$$\left(\frac{\cos^2\theta}{d}\right)^2 * \left(x - d\frac{\sin\theta}{\cos^2\theta}\right)^2 + \left(\frac{\cos\theta}{d}\right)^2 * y^2 = 1 \ [6].$$

This is the classic equation of an ellipse, demonstrating statement (3):

$$\frac{(x-h)^2}{a^2} + \frac{(y-k)^2}{b^2} = 1$$

Supplementary Scheme 4: **The Elliptical Cross Section.**

where a and b are the semi-major and semi-minor axis lengths, and the ellipse is centered in the x-y plane at (h,k). The ellipse described here is centered about the origin along the y axis, and displaced along the x axis by the quantity h:

$$h = d\,\frac{\sin\theta}{\cos^2\theta}\ [7].$$

The semi-major and semi-minor axis lengths are given below in terms of the arbitrary constant d and the angle θ:

$$a = \frac{d}{\cos^2\theta}\ [8],$$
$$b = \frac{d}{\cos\theta}\ [9].$$

All the interesting properties of an ellipse can be described in terms of the quantities a and b. In order to illustrate statements (4) and (5), we will explore 2 such quantities, the distance between the center and the foci, f, and the eccentricity, e, of the ellipse, given by the following equations:

$$f = \sqrt{a^2 - b^2}\ [10],$$
$$e = \sqrt{1 - \left(\frac{b}{a}\right)^2}\ [11].$$

Statement (4), which claims that the paraboloid and the ellipse have a common focus, is true if $h = f$, since the paraboloid focus is at $(0,0)$ and the elliptical foci are located along the x axis at positions $(h$-$f,0)$ and $(h$+$f,0)$. By inserting equation [8,9] into equation [10]:

$$f = \sqrt{\frac{d^2}{\cos^4 \theta} - \frac{d^2}{\cos^2 \theta}}$$

$$f = d \frac{\sin \theta}{\cos^2 \theta} \quad [12].$$

In order to show statement (5), we can similarly insert [8,9] into equation [11]:

$$e = \sqrt{1 - \left(\frac{d}{\cos \theta} * \frac{\cos^2 \theta}{d}\right)^2}.$$

The arbitrary constant d divides out, and the expression reduces quite simply to:

$$e = \sin \theta.$$

General case accounting for SPP dispersion:
The previous reasoning is only exact for structures in which the phase propagation depends only on path length. In that case the interference of isotropic scatterers will be constructive when they are placed on a 3D paraboloid with the emitter at the parabolic focus. This is not exactly the case considered in the manuscript. In this case the phase propagation for radiation in the form of SPPs will be process by a different wave vector than the scattered light, so it is necessary to modify equation [1] by including the wave vectors for the surface plasmon and for air:

$$k_{SPP}\sqrt{x^2 + y^2 + z^2} - k_{air}z = d \ . [13].$$

The arbitrary constant d now represents a constant amount of phase accumulation for the path rather than a distance as in the previous case. We can rewrite equation [13] in the following form:

$$\frac{k_{SPP}^2 - k_{air}^2}{d^2}x^2 + \frac{k_{SPP}^2 - k_{air}^2}{d^2}y^2 + \frac{(k_{SPP}^2 - k_{air}^2)^2}{d^2 k_{SPP}^2}\left(z - d\frac{k_{air}}{k_{SPP}^2 - k_{air}^2}\right)^2 = 1$$

This is no longer the equation of a paraboloid, but an ellipsoid, with one of its foci at the origin. If we use the same rotation of coordinates approach as before, to rotate this ellipsoid an angle θ in the x-z plane, and once again set z to zero, we can write the equation for a new ellipse, now taking into account the appropriate wave vectors.

$$\frac{(k_{SPP}^2 - k_{air}^2 \sin^2 \theta)^2}{d^2 k_{SPP}^2}\left(x + d\frac{k_{air} \sin \theta}{k_{SPP}^2 - k_{air}^2 \sin^2 \theta}\right)^2 + \frac{k_{SPP}^2 - k_{air}^2 \sin^2 \theta}{d^2}y^2 = 1$$

We can once again pick out the important elliptical parameters:

$$h = d \frac{k_{air} \sin \theta}{k_{SPP}^2 - k_{air}^2 \sin^2 \theta}$$

$$a = \frac{d * k_{SPP}}{k_{SPP}^2 - k_{air}^2 \sin^2 \theta}, \qquad b = \frac{d}{\sqrt{k_{SPP}^2 - k_{air}^2 \sin^2 \theta}}$$

$$f = \sqrt{\frac{d^2 k_{SPP}^2}{(k_{SPP}^2 - k_{air}^2 \sin^2 \theta)^2} - \frac{d^2}{k_{SPP}^2 - k_{air}^2 \sin^2 \theta}} = d \frac{k_{air} \sin \theta}{k_{SPP}^2 - k_{air}^2 \sin^2 \theta}$$

$$e = \sqrt{1 - \left(\frac{d}{\sqrt{k_{SPP}^2 - k_{air}^2 \sin^2 \theta}} * \frac{k_{SPP}^2 - k_{air}^2 \sin^2 \theta}{d * k_{SPP}} \right)^2} = \frac{k_{air}}{k_{SPP}} \sin \theta$$

We are ultimately left with the result that the new ellipse is still positioned with the emitter at one focus, since once again $h = f$, and the eccentricity now depends only on θ and the effective index of the SPP mode.
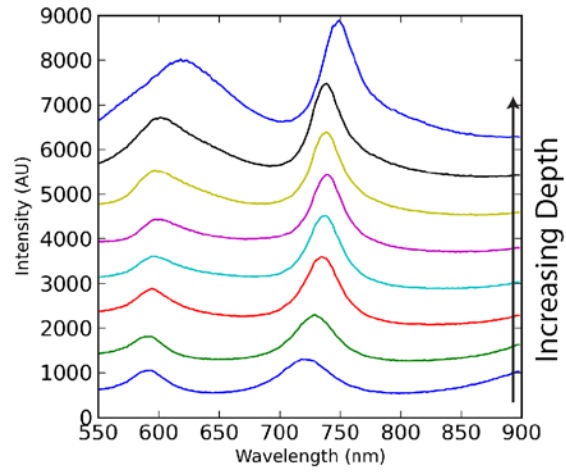
Supplementary Figure 1. **Resonator linewidth versus depth.** Cathodoluminescence spectra collected for arenas with major axis length 1 μm and eccentricity 0.8, for structures with depths ranging from 200 nm to 1 μm. The resonance linewidth increases for increasing depth due to the higher reflectivity of the cavity wall.
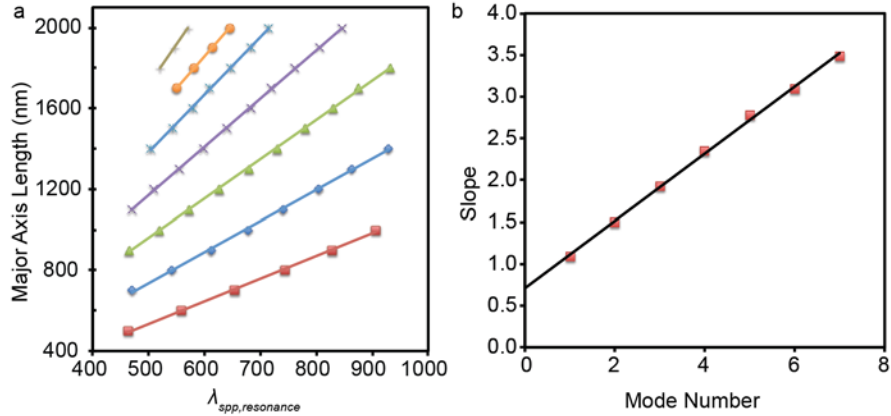
Supplementary Figure 2 **Extraction of the phase pickup on reflection**. **a** Surface plasmon resonant wavelengths versus cavity major axis length for resonators with major axis lengths ranging from 500 nm to 2000 nm, assuming the dispersion relationship for a planar film of gold. A linear relationship between resonator size and the resonant plasmon wavelength is observed, with increasing slope for higher order resonances, in agreement with equation 1. **b** Slope of the lines in **a** for the subsequent modes. A linear increase of the slope with mode number is observed, in agreement with equation 1. The intercept with the ordinate of the line fitted through the data is 0.60, corresponding to a phase shift $\phi = -1.2\pi$.
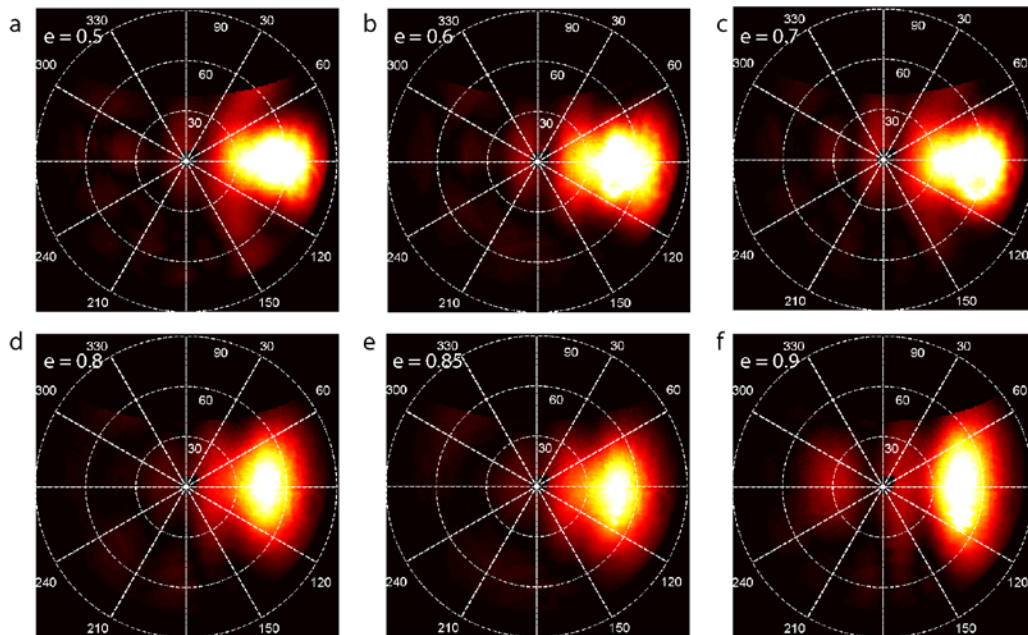
Supplementary Figure 3. **Angular radiation patterns as a function of eccentricity**. Data are shown for structures with a major axis length of 1 μm and eccentricities (indicated in the figures) in the range 0.5-0.9
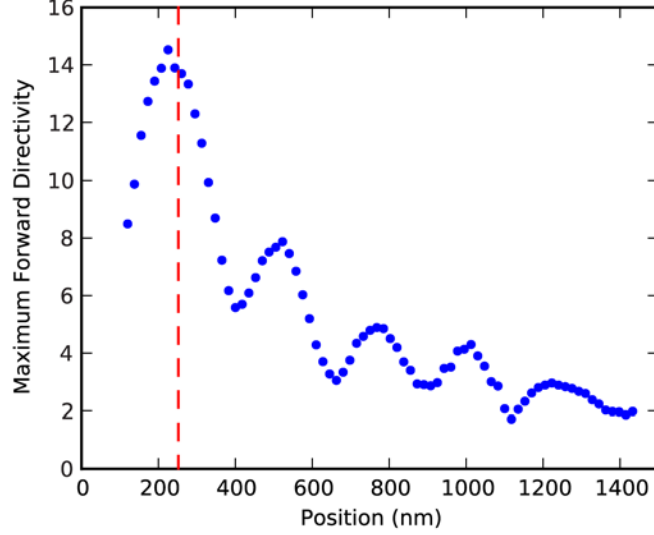
Supplementary Figure 4. **Directivity versus excitation position**. Maximum directivity along the ϕ=90° azimuthal direction (blue circles) as a function of electron beam position along the major axis. The dashed vertical line corresponds to the center position of one of the CL foci (such as *e.g.* in Fig. 1c).

Calculation of Effective Coupling Volume

In the manuscript it is claimed that the effective coupling volume, ie the volume in which an emitter will couple well to the antenna modes, is 100 times larger than that quoted recently for a nanoscale Yagi-Uda antenna. In order to calculate this volume, one need consider the FWHM of the LDOS antinodes parallel and perpendicular to the long axis, as well as the decay of the SPP mode into the air above the plane of the elliptical cavity. As we assumed for calculating the SPP dispersion in the Fabry-Perot model, we here assume the dispersion relationship for the SPPs in the structure to be that for a semi-infinite plane of gold. In this case, the decay length of the SPP into the air is given by following the well-known equation:

$$z_{air} = \frac{\lambda}{2\pi} \left(\frac{|\epsilon'_{metal}| + \epsilon_{air}}{\epsilon_{air}{}^2} \right)^{1/2}$$

We then make the approximation that the volume is a half ellipsoid with semi-axis lengths given by the *x* and *y* HWHM values and the z_{air} given above. For the 1.3 micron ellipse at 600 nm wavelength, the case considered in the paper, these values are 106 nm, 86 nm, and 293 nm, for *x, y* and *z*, respectively, giving a volume of approximately 5.6 x 10⁶ nm³. In contrast, other antennas such as the Yagi-Uda require near-field coupling to a local element, which can only occur when the emitter is placed within a few tens of nanometers from the appropriate position. If we assume this corresponds to a sphere of radius 25 nm, the corresponding coupling volume is 3.27 x 10⁴ nm³, or 171 times smaller than that for the elliptical cavity antenna. In reality, good near-field coupling usually requires even more precise location of the emitter, so the ratio is actually much larger. However, a conservative claim of 100 times is justified.